## PAPER

# Dynamic acoustic field activated cell separation (DAFACS)†

G. D. Skotis,‡[a] D. R. S. Cumming,‡[a] J. N. Roberts,‡[b] M. O. Riehle‡[b] and A. L. Bernassau‡*[a]

Advances in diagnostics, cell and stem cell technologies drive the development of application-specific tools for cell and particle separation. Acoustic micro-particle separation offers a promising avenue for high-throughput, label-free, high recovery, cell and particle separation and isolation in regenerative medicine. Here, we demonstrate a novel approach utilizing a dynamic acoustic field that is capable of separating an arbitrary size range of cells. We first demonstrate the method for the separation of particles with different diameters between 6 and 45 μm and secondly particles of different densities in a heterogeneous medium. The dynamic acoustic field is then used to separate dorsal root ganglion cells. The shearless, label-free and low damage characteristics make this method of manipulation particularly suited for biological applications. Advantages of using a dynamic acoustic field for the separation of cells include its inherent safety and biocompatibility, the possibility to operate over large distances (centimetres), high purity (ratio of particle population, up to 100%), and high efficiency (ratio of separated particles over total number of particles to separate, up to 100%).

## Introduction

Separating and sorting cells and micro-organisms from a heterogeneous mixture is a fundamental step in basic biological,[1] chemical and clinical studies,[2] enabling regenerative medicine, stem cell research, clinical sample preparation, and improved food safety.[3] Biological cell separation needs to enrich a target cell population whilst minimising the presence of unwanted cells or contaminants. At present, the standard systems for cell separation are fluorescently activated cell sorters (FACS) and sedimentation.[4] FACS requires fluorescent labelling, making it complex and expensive, whereas sedimentation has a low ratio of recovery leading to loss of material. As a consequence, there is a considerable demand for the discovery of alternative methods. Microfluidic systems,[5–7] e.g. deterministic sorting,[8] inertial microfluidics,[9] dielectrophoretic,[10] and ultrasonic devices,[11–15] present viable routes to superior

technologies for cell sorting. Techniques utilising ultrasonics are particularly valuable because of the potential for efficient sorting of relatively large microfluidic volumes in a robust, harmless and scalable technology.

Ultrasonic forces are non-invasive and can effectively manipulate cells for applications such as medium exchange,[16] sample concentration,[17–19] sorting,[15,20] enhanced bio-detection and immuno-assays. Achieving cell separation[21] utilizing ultrasonic manipulation by frequency sweeping[11,22] has been previously demonstrated; however, this method has several critical disadvantages. Firstly, unstable forces are generated which leads to differences in the movement of individual trapped particles of the same size or property.[23,24] Secondly, this method exclusively allows small particle displacement, which in turn limits sorting efficiency. Thirdly, frequency sweep sorting inherently lacks flexibility because the frequencies that can be used are limited by the types and dimensions of the transducers. Finally, the dimensional properties of the whole resonator may pose some constraints on the frequency regime.

An alternative to manipulating acoustic frequency is to control the signal phase; it has been demonstrated that shifting the phase of acoustic travelling waves can be used to control the position of micro-particles suspended in an aqueous medium.[25] When two opposing transducers are excited, a linear interference pattern of nodes and antinodes is formed in the interstitial media. The micro-particles are trapped at the minima of the potential acoustic energy density.[26] Electronically shifting the excitation phase of one of the

[a] *School of Engineering, University of Glasgow, Glasgow, G12 8LT, UK. E-mail: Anne.Bernassau@glasgow.ac.uk*
[b] *Centre for Cell Engineering, Institute for Molecular, Cell and Systems Biology, CMVLS, University of Glasgow, Glasgow G12 8QQ, UK*

transducers, with respect to the other, proportionally translates the linear interference pattern in the direction of the added phase delay. The shift of the node position translates to a change in the position of the trapped micro-particles.[27,28]

The new technique devised utilizes a dynamic acoustic field (DAF) with a time-varying phase delay between two opposing travelling waves that results in the separation of particles or cells over large distances (of the order of centimetres). The method shows a high degree of separation selectivity and throughput, making it suitable for applications such as cell sorting. The forces generated by this method are very stable,[23] allowing better spatial separation (improved control and manipulation) of particles and cells to be achieved and maintained compared to results realized using frequency sweeping. This ultimately results in separation of sub-populations in the sample volume with much higher purity.

In this paper, we demonstrate that the flow-less DAF method can be used to separate particles within a sample volume depending on their size or density. We also study the discriminative ability of the method for particles of different sizes or densities. The application of DAF to primary pig dorsal root ganglion neurons as a contact-less means of separating these neurons from debris and smaller cells, which results from tissue digestion, is demonstrated.

## Experimental results and discussion

Initial experiments were conducted with synthetic particles of various sizes and densities in order to demonstrate the feasibility of the approach. Previous studies have found that these particles are a reasonable surrogate for biological cells.[29] Once DAF had been successfully used to discriminate within heterogeneous mixture particles by their sizes and densities in multiple cycles, we progressed to show the capacity of DAF to isolate dorsal root ganglion cells from a mixture of cells and debris as it develops during tissue digestion.

### Principle of operation

The time variant primary acoustic force combined with the viscous force enables one to discriminate particles according to their physico-mechanical properties (size and density). The acoustic force $F_a$, eqn (4), is dependent on the particle radius and particle density. Smaller or less dense particles and cells experience a lower acoustic force $F_a$, with respect to larger or denser particles and cells; therefore, particles and cells of different sizes and different densities will separate. This outlines the fundamental concept utilising the DAF method.

The technique relies on a repeated cycling pattern of the phase difference between two excited transducers from 0° to 360°. Within each cycle, the phase is swept completely through 360° over a time $t_{ramp}$ and then allowed to rest for a period $t_{rest}$ before commencing the next cycle. The interplay between the rate at which the phase is swept and the length of the rest time is at the core of the separation technique.

During $t_{ramp}$, under the correct conditions, the particles of interest experience a strong acoustic force compared to the viscous force.

For a system with particles trapped in one of many nodes, $N$, the particles of interest closely follow the node that traps them and travel from the initial position of the node $N_i$ to the initial position of the next node $N_{i+1}$ (Fig. 2 and 3). This controlled manipulation occurs since a phase shift of 360° moves each node exactly one integer node position, a distance $\Lambda$ (Fig. 1). If at the end of the $t_{ramp}$ period, the smaller particles have not travelled more than halfway (Fig. 2 and 3) from their initial position of $N_i$ to the next node position $N_{i+1}$, they will relax to their starting position during $t_{rest}$, whereas the particles of interest, which have travelled past the midpoint $N_i$ and $N_{i+1}$, will relax towards the next node position $N_{i+1}$.

The interplay between acoustic force and viscous drag force is at the heart of the discriminating ability of the DAF method with $t_{rest}$ serving as an equilibrating interval, during which particles settle at their nearest nodes before the next
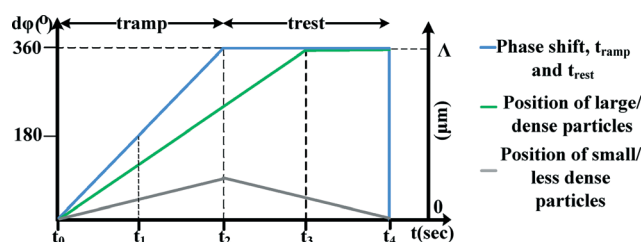


Fig. 1 The effect of the applied phase shift on large and small particles. The large particles move with greater velocity than small particles, thus when the phase shift reaches the rest period at 360° the large particles continue forward and reach the next acoustic node and are trapped. However, the small, light particles relax back to the initial node.
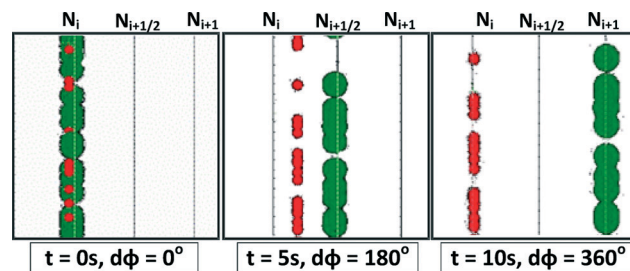


Fig. 2 Particle behaviour under the dynamic acoustic field predicted by the simulation. Under the influence of the phase shift during $t_{ramp}$, the larger (10 μm particle size; in green) and smaller particles (6 μm particle size; in red) separate over time (5 s). The smaller particles are submitted to a smaller acoustic force and thus cannot follow the phase shift, whereas the large particles are moved and slip to the position of the next node ($N_{i+1}$) during $t_{ramp}$. During $t_{rest}$, the larger particles stabilize on the next nodes ($N_{i+1}$), whilst the smaller particles move back to their initial position ($N_i$) and the process can be repeated indefinitely, shifting the larger particles continuously further to the right. The fine vertical lines represent the nodes at $t$.
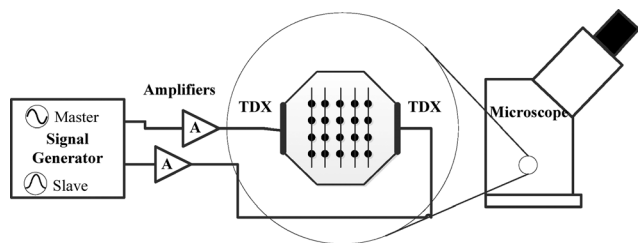
**Fig. 3** Schematic of the experimental setup, with a signal generator (left) driving two opposing ultrasonic transducers (TDX), with a programmable phase shift. The signal was amplified by 10× by two purpose built amplifiers. The octagon well with the transducers was placed on a light microscope for observation.

cycle begins. Assuming the length of $t_{ramp}$ has been selected correctly, the best choice of $t_{rest}$ to achieve cell or particle discrimination depends on the balance between the acoustic force, $F_a$, eqn (4), and the viscous force, $F_v$, eqn (6). $t_{rest}$ and $t_{ramp}$ were measured for different sizes of particles, by applying a step change of 180° in phase to one of the transducers.[25] In water, polystyrene particles of 6, 10 and 45 μm diameters, respectively, require a time delay of 5, 2 and 0.5 s, respectively, to reach their equilibrium positions. This serves as the basis to establish the timescale for $t_{rest}$ and $t_{ramp}$ required to discriminate between particles during the experiments. The DAF method can then be optimized to achieve the optimum separation performance in specific applications. These optimum values of $t_{ramp}$ and $t_{rest}$ are dependent on the viscosity of the medium, as well as the density and size of the particles.

### Acoustic separation simulation

The mechanism of particle separation was studied by using a numerical model to predict the particle behaviour under a dynamic acoustic field. The code was developed in Visual Basic from scratch. We modelled particle behaviour under different dynamic acoustic fields, particle properties (size and density), liquid viscosity and flow. The program sums the forces acting on the particles taking into account the primary acoustic force $F_a$, eqn (4), and the viscous force $F_v$, eqn (6), as a function of time.

The equation of motion of a particle labelled by its position $r(t)$ is given by:

$$\frac{\partial^2 r}{\partial t^2} = \frac{\partial v}{\partial t} = \frac{F_{tot}(r,v,t)}{m} = a(r,v,t) \qquad (1)$$

$F_{tot}$ is the sum of $F_a$ and $F_v$, $m$ is the mass of the particle, and $a$ is the acceleration as a function of particle position $r$ and the relative particle velocity $v$ at time $t$.

These equations of motion are integrated step by step using the Verlet algorithm,[30,31] eqn (2) and (3), to produce the movement of the particles.

$$r(t + \Delta t) = 2r(t) - r(t - \Delta t) + a(t)\Delta t^2 \qquad (2)$$

$$v(t) = \frac{r(t + \Delta t) - r(t - \Delta t)}{2\Delta t} \qquad (3)$$

where $r$ is the particle position, $v$ is its velocity and $\Delta t$ is the integration time step.

The computer program can simulate the movement of $P$ particles among several types of particles differing in their radius and density. Fig. 2 denotes the predicted particle separation of two classes of particles differing in size. The ratio between $t_{ramp}$ and $t_{rest}$ is 1, with a $t_{ramp} = t_{rest} = 5$ s. As predicted, large and small particles are separated.

### Acoustic separation by particle size

To investigate the potential of this method to discriminate particles by size, sets of polystyrene particles (Polysciences Europe, Germany) with varying diameters, (a) 10 and 45 μm and (b) 6 and 10 μm, were subjected to a dynamic acoustic field.

The transducers were excited at a frequency of 4.00 MHz with an amplitude of 8 V$_{pp}$. At this frequency, the wavelength of the sound waves in water is $\lambda = 370$ μm (the velocity of sound velocity in water is 1480 m s$^{-1}$).[32] A schematic of the experimental setup is shown in Fig. 3. The particles agglomerate at the nodes with a separation of $\lambda/2 = \Lambda = 185$ μm.[33,34] To estimate the order of magnitude of the acoustic pressure experienced by the particles of different diameters (6, 10, and 45 μm), we recorded the time taken for the particles to agglomerate at the nodes starting from a randomly distributed motion state. These experiments were repeated 5 times at 5 different locations within the device using time-lapse microscopy. The viscous force, $F_v$, derived from the dimensions and densities of the particles as well as the viscosity of the medium (eqn (6)), allows the acoustic pressure amplitude acting on the particles to be calculated. The acoustic pressure was found to be 91 ± 7 kPa, 62 ± 4 kPa and 48 ± 2 kPa for 6, 10 and 45 μm diameter particles, respectively.

The separation experiments were conducted using two mixtures of particles, each at a particle density of $4.99 \times 10^5$ particles mL$^{-1}$. Mixture A contained 10 and 45 μm diameter particles at a ratio of 1:100. Mixture B contained 6 and 10 μm diameter particles at a ratio of 1:100. At these concentrations, no aggregation of particles was observed. As predicted, the time variant acoustic field was able to manipulate and, at the same time, separate particles according to their size (Fig. 4). Fig. 4a shows the expected behaviour of the large and small particles over time (black = $t_0$, purple = $t_1$, red = $t_2$, yellow = $t_3$) in relation to the initial position of the nodes (indicated by $N_i$ and $N_{i+1}$) and antinodes (indicated by $N_{i+1/2}$) of the acoustic landscape. During $t_{ramp}$, the large particles, experiencing larger acoustic force, follow the moving node and thus can be moved from $N_i$ to $N_{i+1}$. At the same time, smaller particles, experiencing a smaller acoustic force, cannot follow the moving node and thus move over a smaller distance. During $t_{rest}$, the smaller particles return to their initial position $N_i$, while the larger particles settle at the next node $N_{i+1}$. Fig. 4b shows particle traces as a function of time (71 frames covering 36 s). In this case, the 45 μm diameter particles follow the shifted acoustic field (moving towards the right-hand side), while the 10 μm diameter particles stay
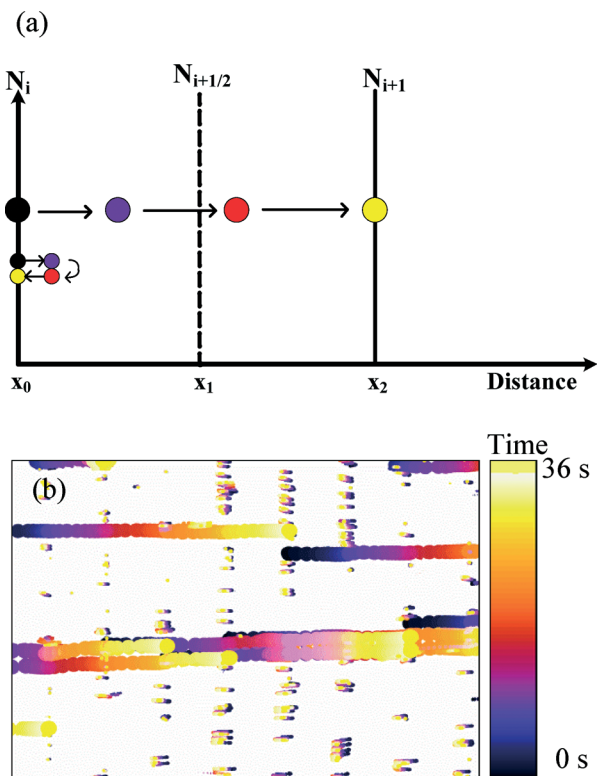
**Fig. 4** Position of the particles as a function of time (represented by colour). (a) A schematic illustration that shows 4 positions of large and small particles. Larger particles, experiencing larger acoustic force, are transported to the next node $N_{i+1}$ at $x_2$, whereas smaller particles, experiencing smaller acoustic force, return to $N_i$ at $x_0$. (b) Experimental data of the 45–10 μm particle mixtures under the dynamic acoustic field (71 frames covering 36 s). The longer trails show the distance traversed by 45 μm diameter particles, whereas the short trails illustrate how 10 μm diameter particles do not traverse the space (see video in the ESI†).



**Fig. 5** Graphs showing (a) the particle density aligned at the nodes and (b) the average particle displacement with time. The large particles, experiencing larger acoustic force, move during $t_{ramp}$ (8 s) and stabilise during $t_{rest}$ (4 s) at the next node resulting in an overall displacement over time. Simultaneously, the small particles, experiencing lower acoustic force, move only slightly, returning to their initial node position during $t_{rest}$. The arrows indicate the relaxing movement during $t_{rest}$. Experiments were repeated 10 times.

close to the position of the original node. The time between frames was 0.5 s. The average movement of small and large particles was 3 ± 1 μm s$^{-1}$ and 30 ± 1 μm s$^{-1}$, respectively, during $t_{ramp}$.

A series of time-lapse images were recorded at regular intervals during separation to produce particle traces. The image stack was then analysed using FIJI[35] and the particle positions were extracted. The resulting data ($x$, $y$, particle area) was used to calculate the efficiency (eqn (7)) and purity (eqn (8)) of separation for each experiment by computing the particle density projected along the node lines and analysing the time variation of this density. Fig. 5a shows the initial position for 10 and 45 μm diameter particles for seven consecutive nodes. Fig. 5b shows the average displacement of the particles for five cycles of continuous phase shift including the rest period. It can be seen that the large particles successively travel during $t_{ramp}$ and stabilise during $t_{rest}$ at the next node resulting in an overall displacement over time. Simultaneously, the small particles move only slightly, therefore not crossing the midpoint of
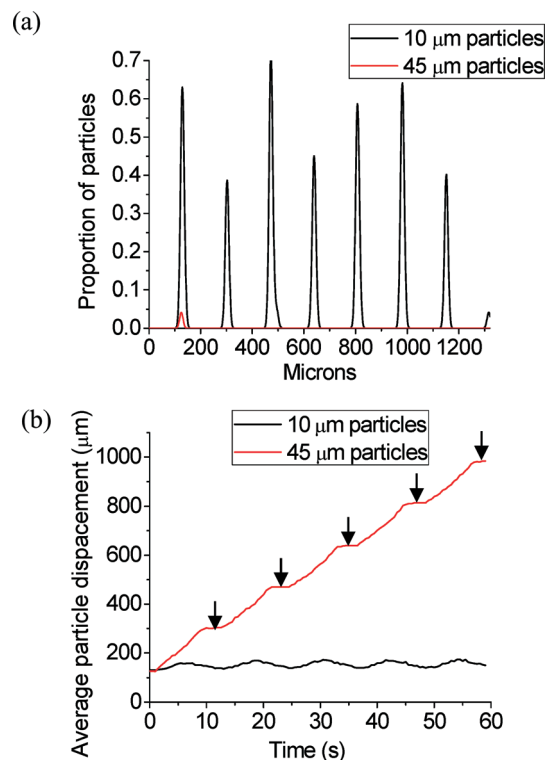
the nodes, and then return to their initial node position during $t_{rest}$.

Separation efficiency was simulated using the DAF model outlined above with the same parameters as the experiments. Table 1(a) shows the simulation results. The regions coloured red represent the parameters that did not show particle separation, whereas the particles were successfully separated in the blue region. Table 1(b) shows the experimental results conducted replicating the simulation parameters. The blue regions represent those parameters where >91% separation was achieved and the red regions represent the parameters where <80% separation was achieved. The yellow regions show those parameters where the separation was 80–90% successful. Comparing computational and experimental results, it can be seen that there is a good match between the simulation and the experimental data.

It can be observed that separation performance improves with $t_{ramp}$ and $t_{rest}$ until it reaches a maximum. This indicates that the acoustic forces that the shifting nodes exert on the particles of interest need a minimum time to overcome inertia and viscous force in order to move the particles from the node $N_i$ to the next node $N_{i+1}$. $t_{ramp}$ is the critical parameter, since it has the greatest effect on the separation result.

**Table 1** (a) Simulation and (b) experimental results for the separation performance, depending the ramp and rest time. Parameters suitable for separation (>0.91 purity) are indicated by a blue shade, and those that are unsuitable are shown in red (purity <80%). Intermediate values are in yellow (purity between 80 and 90%)

(a)

| $t_{rest}$ (s) $t_{ramp}$ (s) | 1.2 | 3.2 | 5.2 | 7.5 | 8.5 |
|---|---|---|---|---|---|
| 3 | | | | | |
| 4 | | | | | |
| 5 | | | | | |
| 6 | | | | | |
| 7 | | | | | |
| 8 | | | | | |
| 9 | | | | | |

(b)

| $t_{rest}$ (s) $t_{ramp}$ (s) | 1.2 | 3.2 | 5.2 | 7.5 | 8.5 |
|---|---|---|---|---|---|
| 3 | 0.40 | 0.69 | 0.60 | 0.61 | 0.69 |
| 4 | 0.50 | 0.59 | 0.74 | 0.90 | 0.78 |
| 5 | 0.68 | 0.70 | 0.79 | 0.90 | 0.78 |
| 6 | 0.62 | 0.72 | 0.76 | 0.89 | 0.76 |
| 7 | 0.57 | 0.98 | 0.92 | 0.97 | 0.97 |
| 8 | 0.99 | 1.00 | 0.95 | 0.95 | 0.95 |
| 9 | 0.98 | 0.91 | 0.95 | 0.98 | 0.91 |

The value of $t_{rest}$ is less influential on the separation of the entities.

When suitable parameters are selected, the separation process reaches its best experimental performance: with the separation ratio achieving ~100% purity and efficiency when $t_{rest}$ = 4 s and $t_{ramp}$ = 8 s.

The simulation and experiment were replicated using 6 and 10 μm diameter particles. For these particles, it was found that ~97% of particles separate, with an efficiency and a purity of ~97%. These results were achieved with a value of $t_{ramp}$ = 15 s and $t_{rest}$ = 15 s. Fig. 6 shows the particle traces as a function of time for 6 and 10 μm diameter particle mixtures (71 frames covering 142 s) under these conditions. The 10 μm diameter particles move from node to node (moving towards the right-hand side), while the smaller particles (6 μm in diameter) remain close to their initial position of the original node. The average movement of the 6 and 10 μm diameter particles was calculated as 2 ± 1 μm s⁻¹ and 10 ± 1 μm s⁻¹, respectively, during $t_{ramp}$.

These above experiments were performed using the smallest gap in size of commercially available particles (10 ± 1 μm and 6 ± 0.6 μm; Polysciences Europe, Germany). Therefore, an experimentally accessible discrimination capability of the acoustic separation device is ±2 μm difference of particle diameter.

**Acoustic separation by particle density**

In this section, particles of the same diameter but of different densities are separated. The acoustic forces are not solely based on particle size but also depend on density (or particle mass), eqn (5). We tested the separation performance against particle density by using 10 μm diameter polystyrene particles and iron-oxide filled particles with a density of $\rho$ = 1.05 g cm⁻³ and $\rho$ = 1.41 g cm⁻³, respectively. The ratio of the concentration of iron-oxide filled and polystyrene particles was 1 : 100.

As for previous experiments, Fig. 7 shows particle traces as a function of time for 10 μm diameter iron-oxide filled and polystyrene particle mixtures using DAF (140 frames
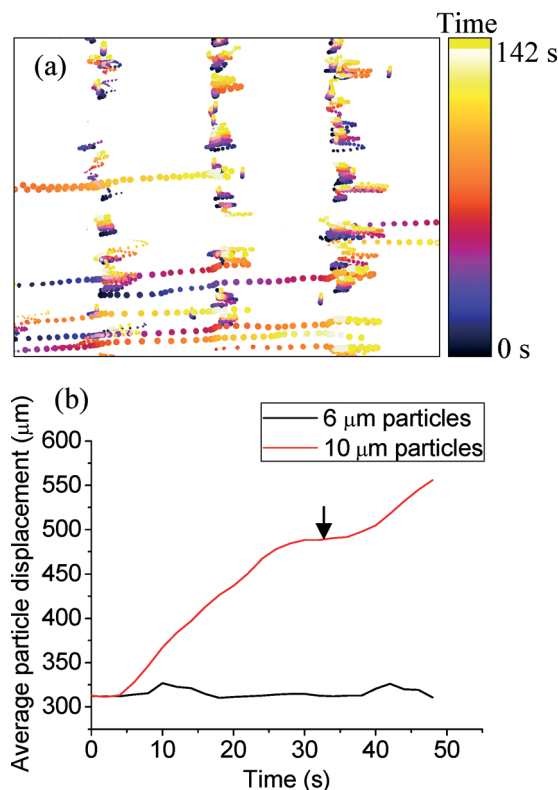


**Fig. 6** (a) Particle traces as a function of time and (b) graph showing the average particle displacement with time. The arrow shows the rest period. The 10 μm particles, experiencing larger acoustic force, move during $t_{ramp}$ (15 s) and stabilise during $t_{rest}$ (15 s) at the next node resulting in an overall displacement over time. Simultaneously, the small particles, experiencing lower acoustic force, move only slightly, returning to their initial node position during $t_{rest}$. The arrows indicate the relaxing movement during $t_{rest}$. Experiments were repeated 5 times.
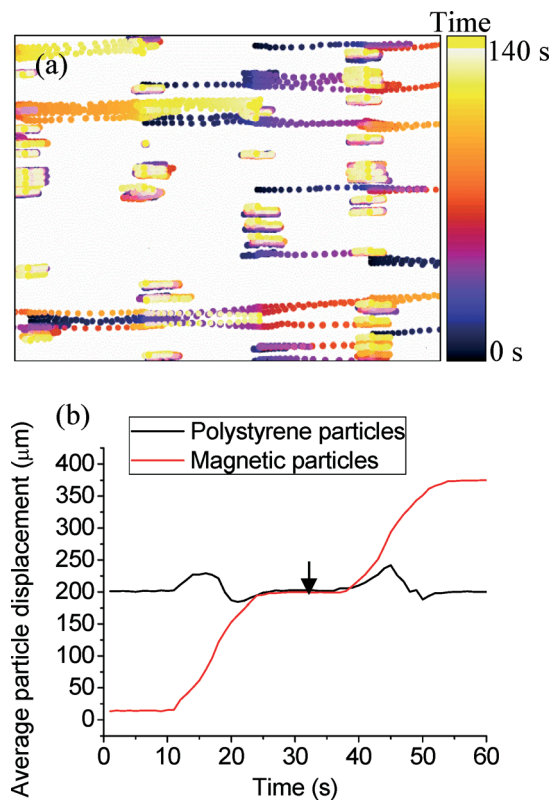
**Fig. 7** (a) Particle traces as a function of time and (b) graph showing the average particle displacement with time. The iron-oxide filled particles, denser and experiencing larger acoustic force, move during $t_{ramp}$ (14 s) and stabilise during $t_{rest}$ (14 s) at the next node resulting in an overall displacement over time. Simultaneously, the polystyrene particles, less dense and experiencing lower acoustic force, move only slightly, returning to their initial node position during $t_{rest}$. The arrows indicate the relaxing movement during $t_{rest}$. Experiments were repeated 5 times.

covering 140 s). It can be seen that the denser particles (iron-oxide filled) are significantly affected by the DAF and continuously travel from left to right, whilst the less dense particles (polystyrene) have a more restricted range of movement close to their starting positions. With these particles, a separation performance of ~99% has been recorded, with an efficiency of ~100% and a purity of ~98% for $t_{ramp}$ = 14 s and $t_{rest}$ = 14 s. The average movement of the polystyrene and iron-oxide filled particles was calculated as $3 \pm 1$ μm s$^{-1}$ and $15 \pm 1$ μm s$^{-1}$, respectively, during $t_{ramp}$.

The less dense particles (polystyrene) experience smaller acoustic force (eqn (4) and (5)) and thus cannot follow the DAF, while the denser particles (iron-oxide filled) track the movement of the dynamic acoustic field. Thus, particles of the same diameter but different densities can be sorted with the DAF method.

## Acoustic separation of dorsal root ganglion (DRG) cells from a heterogeneous medium

As mentioned, particles used in our previous experiments are a reasonable surrogate for biological cells.[29] Since the

acoustic force is proportional to the particle volume, the polystyrene particles are thus likely to experience forces of the same order of magnitude as the cells. At higher intensities, ultrasound can create physiological effects; however, several studies have investigated viability and gene expression at intensities sufficient for manipulation in the MHz range and found no observable detrimental effect on cell viability over extended periods of exposure.[36–39]

To assess a potential practical application, we applied the dynamic acoustic field to separate porcine dorsal root ganglion (DRG) neurons from a freshly isolated mixture containing myelin debris and other non-neuronal cells. The neurons would normally be separated based on their hydrodynamic state using centrifugation across a Ficoll gradient.[40] The DRG neurons have an average size from 17 to 145 μm, while the myelin debris has a size of approximately from 10 to 15 μm.

Fig. 8 shows debris (~26 μm) and a single DRG neuron (~85 μm) in the presence of an acoustic standing wave. These entities aligned themselves in vertical lines, agglomerating at the nodes of the acoustic field.[41] A dynamic acoustic field was then applied (using a $t_{ramp}$ and $t_{rest}$ of 5 s), and the resulting time-lapse overlay is represented in Fig. 9a. The static material does not produce a trace, whereas the material that has been displaced shows a trace that moves from left to right. The DRG cell follows the shifted acoustic field (moving towards the right-hand side), while the debris exhibits minimal displacement of the original node. The time between frames was 0.5 s. The average movement of the DRG cell was calculated to be $18.5 \pm 1$ μm s$^{-1}$ during $t_{ramp}$. Fig. 9b shows the displacement of the DRG over time.

In these experiments, the DRG cells exhibit similar behaviour to the particles in the previous experiments. Only the large DRG neurons are differentially shifted to the right, while smaller cells and debris remain in their original node.
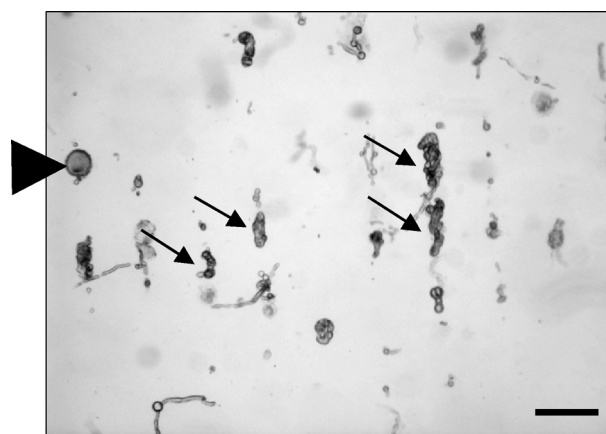


**Fig. 8** Debris (arrows) and a single DRG neuron (arrowhead) in the presence of acoustic standing waves. The cells and debris agglomerate in the nodal line of the acoustic landscape. Scale bar = 185 μm.
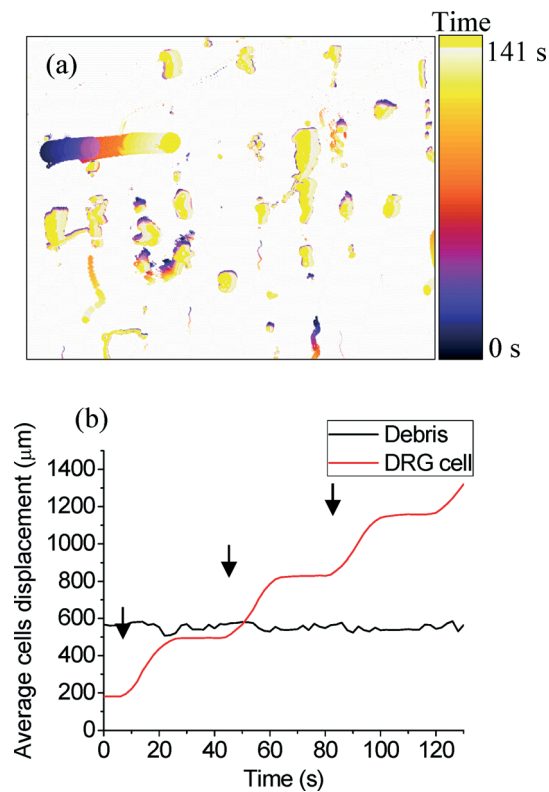
**Fig. 9** (a) Cell traces as a function of time and (b) graph showing the average cell displacement with time. The DRG cell, experiencing larger acoustic force, moves during $t_{ramp}$ (5 s) and stabilises during $t_{rest}$ (5 s) at the next node resulting in an overall displacement over time. Simultaneously, the debris exhibit minimal displacement of the original node. The arrows indicate the relaxing movement during $t_{rest}$. The distance between nodes was 185 μm. Experiments were repeated 4 times.

## Conclusion

We have demonstrated a new technique using a dynamic acoustic field to separate particulate materials on the basis of size and density. Separation occurs as long as the balance of the acoustic forces and the viscous force is differentiated between particle types. Since the acoustic forces are a function of size and density of the particles, many types of particles or cells can be separated. A detailed evaluation has been carried out using polystyrene and iron-oxide filled particles, prior to applying the technique to the separation and purification of recovered dorsal root ganglion cells from the myelin cells. The advantages of DAF for the separation of particles include its inherent safety and biocompatibility, the possibility of operating over large distances (centimetres), the high purity (ratio of particle populations) that can be achieved that is up to 100% and the high efficiency (ratio of separated particles over total number of particles of the same type in the sample) that can be up to 100%.

## Methods

### Acoustic radiation force

The primary acoustic force $F_a$, eqn (4), and viscous force $F_v$, eqn (6), to which the particles are submitted at time $t$ are given by eqn (4) to (6):

$$F_a = -\left(\frac{\pi p_0^2 V_c \beta_w}{2\lambda}\right) \times \varphi(\beta, \rho) \times \sin(2kx) \quad (4)$$

$$\phi(\beta, \rho) = \frac{5\rho_c - 2\rho_w}{2\rho_c + \rho_w} - \frac{\beta_c}{\beta_w} \quad (5)$$

$$F_v = -6\pi\eta R v \quad (6)$$

where $p_0$ is the acoustic pressure amplitude, $V_c$ is the volume of the particle, $\lambda$ is the wavelength, $k$ is the wave number that is equal to $2\pi/\lambda$, $x$ is the distance from a pressure node, $\rho_c$ and $\rho_w$ are the densities of the particle and the fluid, respectively, $\beta_c$ and $\beta_w$ are the compressibility of the particle and the fluid, respectively, $\eta$ is the medium viscosity, $R$ is the particle radius, and $v$ is the relative velocity.

The acoustic contrast factor, eqn (5), represented by $\phi$ in eqn (4), depends on both the particle density ($\rho_c$) and its compressibility ($\beta_c$) in relation to the corresponding properties of the surrounding medium ($\rho_w$, $\beta_w$). The equation of the primary radiation force, $F_a$, eqn (4), states that the acoustic force applied on the particles is proportional to the acoustic pressure amplitude ($\rho_0$) squared and to the volume of the particles ($V_c$). The acoustic dynamic field takes advantage of the size dependency of the mechano-physical properties of the micro-entities being sorting, that scales with particle volume, inducing a primary force which is strongly dependent on particle size ($r^3$) and medium viscosity.

### Acoustic device

The acoustic device, described elsewhere,[25] has been used to demonstrate how the dynamic acoustic field technology can be applied to particle sorting. In this paper, only two opposite transducers were used. The pair of transducer was synchronised using an arbitrary waveform generator (TGA12104, Thurlby Thandar Instruments, UK) allowing independent control of the amplitude, phase and frequency of each channel. The waveform generator was controlled by a general purpose interface bus (GPIB) utilizing a script written in Labview (National Instruments, USA). The signals, created by the waveform generator, were amplified and matched by high-speed buffers (AD811 Analog Devices USA; BUF634T, Texas Instruments, USA), before being fed to the transducers *via* length matched coax cables.

Furthermore, an agar layer was introduced into the device to minimize the streaming[42] and maximize the precision in control of the particle movement.

### Separation performance

We studied the separation performance in terms of purity and efficiency depending on the ramping time and the resting time of the phase. Separation purity and separation efficiency are two figures of merit that can used to assess separation performance. The separation purity and efficiency can be expressed as:

$$\text{Efficiency} = \frac{\text{Target cells in desired area}}{\text{Total target cells in sample}} \times 100\% \qquad (7)$$

$$\text{Purity} = \frac{\text{Target cells in desired area}}{\text{Total cells in desired area}} \times 100\% \qquad (8)$$

The demonstrated results in Table 1 were calculated using the following formula which is the average of purity and efficiency as described above:

$$\text{Final grade} = \frac{\text{Efficiency} + \text{Purity}}{2} \qquad (9)$$

## Competing financial interests

The authors declare no competing financial interests.

## Acknowledgements

## References

1 Diethard Mattanovich and Nicole Borth, *Microb. Cell Fact.*, 2006, **5**(1), 12.
2 Dimitri Pappas and Kelong Wang, *Anal. Chim. Acta*, 2007, **601**(1), 26.
3 S. Neethirajan, I. Kobayashi, M. Nakajima, D. Wu, S. Nandagopal and F. Lin, *Lab Chip*, 2011, **11**(9), 1574.
4 R. G. Miller and R. A. Phillips, *J. Cell. Physiol.*, 1969, **73**(3), 191.
5 Yan Gao, Wenjie Li and Dimitri Pappas, *Analyst*, 2013, **138**(17), 4714.
6 A. Lenshof and T. Laurell, *Chem. Soc. Rev.*, 2010, **39**(3), 1203.
7 Y. Chen, P. Li, P.-H. Huang, Y. Xie, J. D. Mai, L. Wang, N.-T. Nguyen and T. J. Huang, *Lab Chip*, 2014, **14**(4), 626.
8 J. A. Davis, D. W. Inglis, K. J. Morton, D. A. Lawrence, L. R. Huang, S. Y. Chou, J. C. Sturm and R. H. Austin, *Proc. Natl. Acad. Sci. U. S. A.*, 2006, **103**(40), 14779.
9 A. A. S. Bhagat, S. S. Kuntaegowdanahalli and I. Papautsky, *Microfluid. Nanofluid.*, 2009, **7**(2), 217.
10 A. Valero, T. Braschler, N. Demierre and P. Renaud, *Biomicrofluidics*, 2010, **4**(2), 022807.
11 N. Harris, R. Boltryk, P. Glynne-Jones and M. Hill, *Phys. Procedia*, 2010, **3**(1), 277.
12 L. Schmid, D. A. Weitz and T. Franke, *Lab Chip*, 2014, **14**(19), 3710.

13 O. Jakobsson, C. Grenvall, M. Nordin, M. Evander and T. Laurell, *Lab Chip*, 2014, **14**(11), 1943.
14 X. Ding, S.-C. S. Lin, M. I. Lapsley, S. Li, X. Guo, C. Y. Chan, I. K. Chiang, L. Wang, J. P. McCoy and T. J. Huang, *Lab Chip*, 2012, **12**(21), 4228.
15 X. Ding, Z. Peng, S. C. Lin, M. Geri, S. Li, P. Li, Y. Chen, M. Dao, S. Suresh and T. J. Huang, *Proc. Natl. Acad. Sci. U. S. A.*, 2014, **111**(36), 12992.
16 J. J. Hawkes, R. W. Barber, D. R. Emerson and W. T. Coakley, *Lab Chip*, 2004, **4**(5), 446.
17 M. Hill, Y. Shen and J. J. Hawkes, *Ultrasonics*, 2002, **40**(1–8), 385.
18 D. Carugo, T. Octon, W. Messaoudi, A. L. Fisher, M. Carboni, N. R. Harris, M. Hill and P. Glynne-Jones, *Lab Chip*, 2014, **14**(19), 3830.
19 M. Nordin and T. Laurell, *Lab Chip*, 2012, **12**(22), 4610.
20 F. Petersson, A. Nilsson, C. Holm, H. Jonsson and T. Laurell, *Analyst*, 2004, **129**(10), 938.
21 A. H. J. Yang and H. T. Soh, *Anal. Chem.*, 2012, **84**(24), 10756.
22 Yang Liu and Kian-Meng Lim, *Lab Chip*, 2011, **11**(18), 3167.
23 T. Kozuka, T. Tuziuti, H. Mitome, F. Arai and T. Fukuda, in *Micromechatronics and Human Science, 2000. MHS 2000. Proceedings of 2000 International Symposium on (IEEE, 2000)*, p. 201.
24 T. Kozuka, T. Tuziuti, H. Mitome and T. Fukuda, in *Micro Machine and Human Science, 1995. MHS '95, Proceedings of the Sixth International Symposium on (IEEE, 1995)*, p. 179.
25 A. L. Bernassau, C. R. P. Courtney, J. Beeley, B. W. Drinkwater and D. R. S. Cumming, *Appl. Phys. Lett.*, 2013, **102**(16), 164101.
26 A. Bernassau, P. MacPherson, J. Beeley, B. W. Drinkwater and D. Cumming, *Biomed. Microdevices*, 2013, **15**(2), 289.
27 A. L. Bernassau, O. Chun-Kiat, M. Yong, P. G. A. Macpherson, C. R. P. Courtney, M. Riehle, B. W. Drinkwater and D. R. S. Cumming, *IEEE Trans. Ultrason. Ferroelectr. Freq. Control*, 2011, **58**(10), 2132.
28 C. R. P. Courtney, C. K. Ong, B. W. Drinkwater, A. L. Bernassau, P. D. Wilcox and D. R. S. Cumming, *P. R. Soc. A*, 2012, **468**, 337.
29 J. Shi, D. Ahmed, X. Mao, S.-C. S. Lin, A. Lawit and T. J. Huang, *Lab Chip*, 2009, **9**(20), 2890.
30 L. Verlet, *Phys. Rev.*, 1968, **165**(1), 201.
31 L. Verlet, *Phys. Rev.*, 1967, **159**(1), 98.
32 M. Baumann, V. Daanen, A. Leroy and J. Troccaz, in *Computer Vision Approaches to Medical Image Analysis*, ed. R. R. Beichel and M. Sonka, Springer, Berlin/Heidelberg, 2006, vol. 4241, p. 248.
33 T. Laurell, F. Petersson and A. Nilsson, *Chem. Soc. Rev.*, 2007, **36**(3), 492.
34 T. Kozuka, T. Tuziuti, H. Mitome and T. Fukuda, in *Micro Machine and Human Science, 1994. Proceedings, 1994 5th International Symposium on (IEEE, 1994)*, p. 83.
35 J. Schindelin, I. Arganda-Carreras, E. Frise, V. Kaynig, M. Longair, T. Pietzsch, S. Preibisch, C. Rueden, S. Saalfeld, B. Schmid, J. Y. Tinevez, D. J. White, V. Hartenstein,

K. Eliceiri, P. Tomancak and A. Cardona, *Nat. Methods*, 2012, **9**(7), 676.

36 H. Bohm, P. Anthony, M. R. Davey, L. G. Briarty, J. B. Power, K. C. Lowe, E. Benes and M. Groschl, *Ultrasonics*, 2000, **38**(1), 629.

37 D. Bazou, R. Kearney, F. Mansergh, C. Bourdon, J. Farrar and M. Wride, *Ultrasound Med. Biol.*, 2011, **37**(2), 321.

38 B. Vanherberghen, O. Manneberg, A. Christakou, T. Frisk, M. Ohlin, H. M. Hertz, B. Onfelt and M. Wiklund, *Lab Chip*, 2010, **10**(20), 2727.

39 Hultstrom, O. Manneberg, K. Dopf, H. M. Hertz, H. Brismar and M. Wiklund, *Ultrasound Med. Biol.*, 2007, **33**(1), 145–151.

40 R. Gilabert and P. McNaughton, *J. Neurosci. Methods*, 1997, **71**(2), 191.

41 F. Gesellchen, A. L. Bernassau, T. Dejardin, D. R. S. Cumming and M. O. Riehle, *Lab Chip*, 2014, **14**(13), 2266.

42 A. L. Bernassau, P. Glynne-Jones, F. Gesellchen, M. Riehle, M. Hill and D. R. S. Cumming, *Ultrasonics*, 2014, **54**(1), 268.